LBNL-42218
Preprint

ERNEST ORLANDO LAWRENCE
BERKELEY NATIONAL LABORATORY

Realizing the Benefits of Restored Periodicity in a Particle Storage Ring

D. Robin, J. Safranek, and W. Decking

Advanced Light Source Division

August 1998

Submitted to
Physics Review E

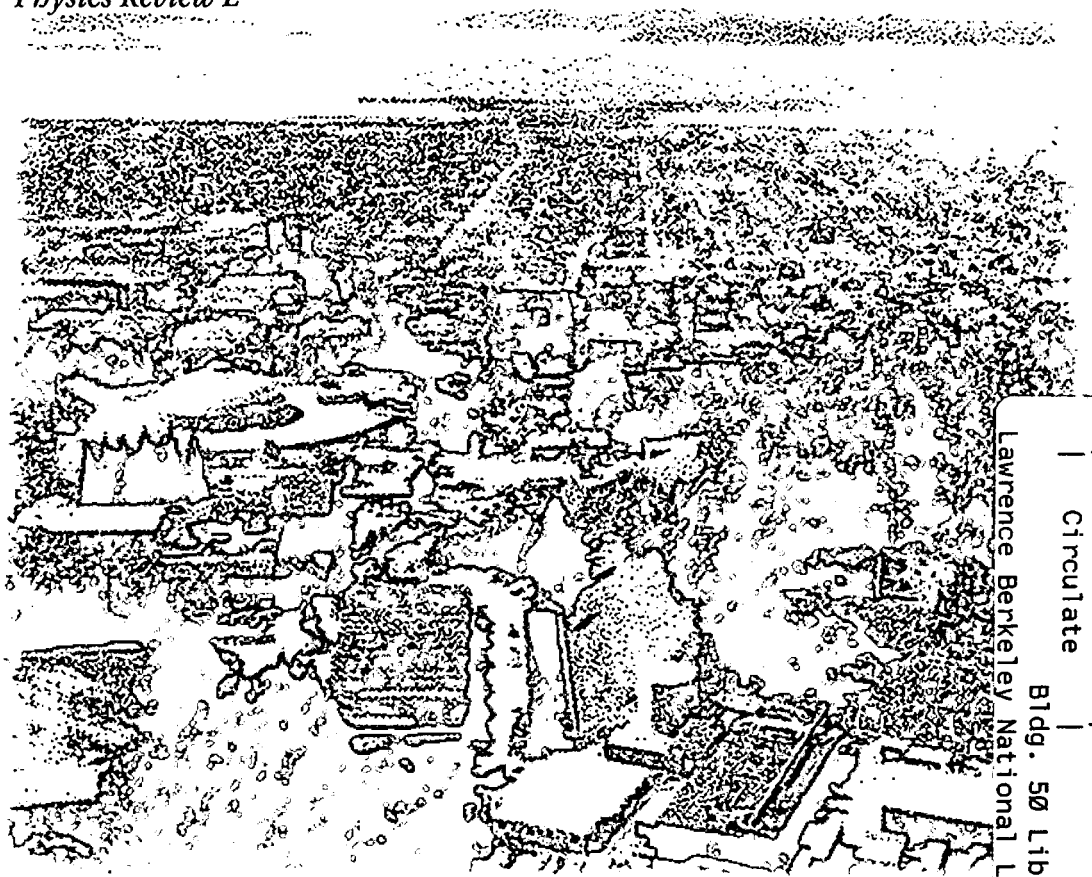

DISCLAIMER

LBNL-42218

Realizing the Benefits of Restored Periodicity in a Particle Storage Ring

D. Robin,[1] J. Safranek,[2] and W. Decking[1]

[1]Advanced Light Source Division
Ernest Orlando Lawrence Berkeley National Laboratory
University of California
Berkeley, CA 94720

[2]Stanford Linear Accelerator Center
Stanford, CA 94309

August 1998

This work was supported by the Director, Office of Science, Office of Basic Energy Sciences, Materials Sciences Division, of the U.S. Department of Energy under Contract No. DE-AC03-76SF00098.

LBNL-42218

REALIZING THE BENEFITS OF RESTORED PERIODICITY IN A PARTICLE STORAGE RING

D. Robin
Advanced Light Source
Lawrence Berkeley National Laboratory
Berkeley, CA 94720

J. Safranek
Stanford Linear Accelerator Center
Stanford, CA 94309

W. Decking
Advanced Light Source
Lawrence Berkeley National Laboratory
Berkeley, CA 94720

August 28, 1998

*This work was supported by the Director, Office of Energy Research, Office of Basic Energy Sciences, Materials Sciences Division of the U.S. Department of Energy, under Contract No. DE-AC03-76SF00098

Realizing the Benefits of Restored Periodicity in a Particle Storage Ring

D. Robin

Lawrence Berkeley National Laboratory

Berkeley, CA 94720

J. Safranek

Stanford Linear Accelerator Center

Stanford, CA 94309

W. Decking

Lawrence Berkeley National Laboratory

Berkeley, CA 94720

(August 28, 1998)

Abstract

An essential feature of third generation storage ring based light sources is the magnetic lattice is designed with a high degree of periodicity. Tracking simulations show that if the periodicity is perturbed (by focusing errors for example), non-linear resonances become excited, which causes a reduction in the dynamic aperture. Therefore it is important to have a method to measure and correct perturbed periodicity. In this paper we study the effect of broken and restored periodicity at an actual third generation light source: the Advanced Light Source at Lawrence Berkeley National Laboratory. First we show that it is possible to accurately determine the storage ring optics and thus the perturbation of the periodicity by fitting measured orbit response

matrices. This method allows us to determine individual field gradient errors in quadrupoles and closed orbit errors in sextupoles. By varying individual quadrupole field strengths it is possible to correct the optics, largely restoring the lattice periodicity. A comparison is made of the performance of the storage ring before and after the optics are corrected. Measurements of the injection show large improvements in efficency after the optics are corrected. Also measurements of the electron beam tails and the synchrotron light image reveal a large suppression in resonance excitation after the optics are corrected.

29.27.Bd, 29.27.Fh, 29.20.Dh

I. INTRODUCTION

The Advanced Light Source (ALS) is a 1.0 to 2.0 GeV storage ring based synchrotron light source located at Lawrence Berkeley National Laboratory [1]. Similar to other third generation light sources, the ALS storage ring was designed to produce small beam emittances to increase the brightness of radiation emitted from insertion devices. The small beam emittances are created by strongly focusing the beam with high field quadrupole magnets. These quadrupole magnets generate large chromatic aberrations that need to be corrected with high field sextupole magnets. These sextupole magnets in turn introduce geometrical and higher order chromatic aberrations that can result in undesirable dynamic behavior of the electrons – such as excitation of structural resonances and chaotic motion. This nonlinear behavior can lead to:

1. Small dynamic aperture
    (a) Short lifetimes (Touschek and gas-scattering)
    (b) Slow injection rates
2. Distortion in the beam shape
3. Reduction in the betatron tune space where beam can stably circulate

There is an important feature of the ring design that helps suppress resonance excitation — the ring is designed with a high degree of periodicity. The ALS ring is 12-fold periodic. Fig. 1 shows one twelfth of the ring consisting of 3 dipole magnets (B) 6 quadrupoles (QF, QD and QFA) and 4 sextupole magnets (SF and SD). The locations of horizontal and vertical steering magnets, and beam position monitors (BPMs) are also shown. The dipole magnets have quadrupole fields in addition to their dipole fields (i.e., combined function magnets). The magnetic lattice is a triple bend achromat that is mirror symmetric about its center.

Ideally each of the 12 sectors is identical. In such a ring, structural betatron resonances may occur when the following condition is satisfied

$$N_x \frac{\nu_x}{12} + N_y \frac{\nu_y}{12} = M \tag{1}$$

where ν_x and ν_y are the horizontal and vertical betatron tunes for the full ring and N_x, N_y, and M are integers. In a ring with no periodicity the full ring is the basic unit of the machine. In that case structural betatron resonances may occur when

$$N_x\nu_x + N_y\nu_y = M \tag{2}$$

which is much less restrictive than the condition given by equation 1.

In this paper we define the resonance conditions given in equation 1 as resonances that are "allowed" by periodicity. All conditions given in equation 2, excluding those that are given in equation 1, we define as resonances that are "unallowed" by periodicity. To illustrate the reduction in the number of low-order resonances with 12-fold periodicity, all resonances up to fifth order ($|N_x| + |N_y| \leq 5$) are plotted in the left side of Fig. 2 and the allowed resonances up to fifth order are plotted in the right side of Fig. 2.

Unallowed resonances are excited when focusing errors, such as quadrupole field errors and orbit errors in sextupoles, perturb the periodicity of the ring. The strength of resonance excitation depends upon the degree of periodicity breaking. The periodicity is broken to some extent in every storage ring. In practice we would like to know:

1. Can we identify the cause of the periodicity breaking?
2. How bad is the periodicity broken?
3. Can we restore the periodicity?
4. How is the beam dynamics affected by the broken periodicity?
5. How is the beam dynamics improved by the restored periodicity?

Through experimental studies we were able to answer these questions. In this paper we present the results of the studies. In Sec. II we describe the technique of modeling measured orbit response matrix data that was used to determine the cause of periodicity breaking. We present the results of our modeling to find individual quadrupole gradient errors (Sec. III) and horizontal orbit offsets in sextupoles (Sec. IV). These errors are responsible for a 6% horizontal and a 19% vertical rms variation in the ring's β-function. This β-beating

was used as a measure of broken periodicity. In Sec. V we describe how the linear optics were corrected and the ring's periodicity was restored by adjusting individual quadrupole gradients in the ring. After the optics were corrected, the horizontal and vertical β-beating was reduced to less than 1%.

In Sec. VI and Sec. VII we compare the performance of the storage ring before and after the optics were corrected. The storage ring with corrected optics has much higher injection efficiency. We also measured a reduction in the strength of the unallowed resonance excitation. In Sec. VIII we end with some concluding remarks.

II. FITTING THE MODEL

The magnet gradient distribution in the ALS was determined by analyzing measured orbit response matrix data. The analysis method is one suggested by Corbett, Lee and Ziemann at SLAC [2] and refined by Safranek at BNL [3,4]. The first analysis of ALS orbit response matrices was made in 1994 shortly after commissioning by Bengtsson and Meddahi [5] and later by Robin et al [6].

An orbit response matrix, $\mathbf{M}$, is defined by

$$\begin{pmatrix} \vec{x} \\ \vec{y} \end{pmatrix} = \mathbf{M} \begin{pmatrix} \vec{\theta}_x \\ \vec{\theta}_y \end{pmatrix} \tag{3}$$

where $\vec{\theta_x}$, $\vec{\theta_y}$ are changes in steering magnet strengths and $\vec{x}$, $\vec{y}$ are the resulting electron orbit perturbations at the beam position monitors (BPMs). The measured orbit response matrix, $\mathbf{M}_{meas}$, is obtained by changing a steering magnet and measuring orbit changes with BPMs. Also it is possible to calculate the orbit response matrix, $\mathbf{M}_{mod}$, assuming some gradient distribution in the storage ring and using an optics model. If the assumed gradient distribution is wrong then $\mathbf{M}_{meas}$ and $\mathbf{M}_{mod}$ will not be the same. The actual gradient distribution in the ring is then determined by adjusting the gradient distribution in the model to minimize the difference between $\mathbf{M}_{meas}$ and $\mathbf{M}_{mod}$. To calculate $\mathbf{M}_{mod}$ we used the optics code COMFORT [7].

The parameters in the COMFORT model were varied to minimize the χ^2 deviation between the model and measured orbit response matrices using the computer code LOCO [4]:

$$\chi^2 = \sum_{i,j} \frac{(M_{mod\ ,ij} - M_{meas\ ,ij})}{\sigma_i^2} \tag{4}$$

where the summation is over the BPMs, i, and the steerers, j. The σ_i are the measured rms noise levels for the BPMs. In the ALS there are 94 horizontal correctors, 70 vertical correctors, 96 horizontal and 96 vertical BPMs. This means that there are (96 + 96) x (94 +70) = 31488 elements in the fully coupled matrix or (94 x 96) + (70 x 96) = 15744 elements in the uncoupled matrix. In this work we did not attempt to determine the skew gradient components in the ring. Therefore we ignore the cross terms in the matrix and only fit the uncoupled matrix elements.

If the beam orbit is not steered horizontally through the center of the sextupoles there is a quadrupole feeddown component of the sextupole field proportional to both the horizontal offset and the integrated strength of the sextupole. At the ALS it is possible to store beam and measure an orbit response matrix with the sextupole magnets turned off. This is convenient because it allows us to fit that matrix without varying the sextupoles' quadrupole gradients. In that way we are able to find the quadrupole gradients independently of the sextupoles. Then we measure an orbit response matrix with the sextupoles turned on and fit the data by varying the sextupole gradients with the quadrupole gradients kept fixed in the model. In this way we are able to minimize the number of parameters used to fit each response matrix. So in gathering the data we make a back to back measurement of two response matrices; one with the sextupoles turned off and another with the sextupoles turned on.

First we discuss the gradient parameters used to fit the data set with the sextupole magnets turned off. There are 108 magnets in the storage ring that have quadrupole components: 36 Bs, 24 QFs, 24 QDs, and 24 QFAs (see Fig. 1). These magnets are powered by 50 power supplies: One supply powers all the Bs, one supply powers all QFAs, and the

remaining 48 supplies individually power the 24 QF and 24 QD magnets. In our fit we only varied 50 quadrupole field strengths, one associated with each of the quadrupole supplies. We did not choose to vary all 108 parameters for two reasons. First the noise of the data is not sufficiently small to accurately distinguish gradient errors in all individual magnets. Second we assume that gross quadrupole errors would most probably be due to differences in power supplies and not to mechanical differences in the magnets [8].

The parameters used to fit the data set with the sextupoles turned off are the quadrupole field strengths (50), the BPM gains (192), and the steerer magnets gains (164). In addition there is another set of parameters used in the fit: the energy shifts associated with changes in steerer magnets. This energy shift occurs when the field of a horizontal steerer magnet located in a dispersion region is changed [9]

$$\frac{\Delta \mathrm{E}}{E} = -\frac{\theta_x \eta_x}{\alpha \mathrm{L}_0} \tag{5}$$

where θ_x is the change in steerer magnet strength, η_x is the dispersion at the location of the steerer magnet, α is the momentum compaction, and L_0 is the circumference of the ring. This adds another 94 parameters to the fit. A total of 500 parameters are varied to minimize χ^2.

After we fit the response matrix data, we fit the response matrix data set taken with the sextupoles turned on. The chromaticity is adjusted using 2 families of sextupoles, SF and SD. To fit this data we fix the values for the quadrupoles that we calculated from the previous set and only vary quadrupole gradients associated with each of the 24 SF and 24 SD sextupole magnets. In addition to the 48 quadrupole gradients we vary the 192 BPM gains, 164 corrector gains, and the 94 energy shifts. So in the second iteration there are 498 parameters that are varied to minimize χ^2. For more details concerning the LOCO fit we refer the reader to another paper [4].

III. QUADRUPOLE FIELD ERRORS

Initial LOCO analyzes of the ALS storage ring were made in the fall of 1995. To generate the measured response matrix the magnitude of the steerer magnet changes were chosen to produce approximately a 0.8 mm rms change horizontally and a 1 mm rms change vertically in the orbit at the BPMs. The initial LOCO analysis was made for quadrupoles without the sextupole magnets turned on. Before the fit the disagreement between the measured and modeled orbit changes is greater than $100\mu m$ rms horizontally and vertically. After fitting the model the agreement between the measured and modeled orbit changes is $13\mu m$ rms horizontally and vertically. This should be compared with the measured rms noise of the BPMs, σ_i, which was $12\mu m$ horizontally and $10\mu m$ vertically. Therefore the fits nearly converged down to the noise. An example of the agreement between the model and machine for a typical orbit change before and after the fit can be seen in Fig. 3.

Although the accuracy of the method is difficult to determine, there was only a 0.1% rms variation in the fit quadrupole gradients from data set to data set. Table I shows the variation in field strengths among the members of the two families of quadrupoles that are powered with individual power supplies. As seen in the table, the QD family has significantly larger variation in field than the QF family. These QD values are particularly large when compared with the quadrupole design tolerances which specify that within a family the field variation should lie within a band of $\pm$ 0.2% [10].

As mentioned in the previous section we assumed that any large variation in quadrupole fields is more likely a result of the variation in the power supply than in the mechanical construction. Independently each magnet power supply excitation current was measured using a hand held current monitor [11]. A magnet-to-magnet comparison was made between the quadrupole strengths obtained with the current meter and the response matrix fitting. The results are shown in Fig. 4. The agreement is within the precision of the current monitor ($\pm$ 0.3%). In fact the rms difference between the two measurements is 0.2%. Since these two independent measurement methods produced consistent results, it gave us confidence

that the two methods are capable of pinpointing individual magnet field strength errors to a precision better than 0.3%. In particular, both measurements showed that 4 of the 24 QD magnets were more than 1% lower than the average (magnets 9, 13, 16, and 22 in Fig. 4). It was ultimately shown that the reason that power supplies were not regulating to specification was due to malfunctioning regulating shunts.

Without sextupoles we identified the major cause of periodicity breaking thus answering the first question posed in the introduction. The second question posed was how bad the periodicity was broken. One measure of the periodicity breaking is the distortion of the β-function in the ring. Using the calibrated model it is possible to compute the β-function. The rms perturbation of the β-function from the ideal β-function is 3% horizontally and 15% vertically. The perturbation of the β-function is displayed in Fig. 5.

In 1996 we improved the quality of our measured response matrices. Prior to 1996 only one measurement of the orbit was taken after each steering magnet was changed. To reduce the noise level of the BPMs, 500 measurements of the orbit were taken after each steering magnet was changed. These 500 orbits were then averaged. As expected the noise level was reduced by the square root of the number of averages from greater than 10 μm to less than 1 μm. At the time of this paper the agreement between the measured and the modeled response matrices are 4 μm horizontally and vertically. The fits still do not converge down to the noise level.

We are not completely sure of the reason, but one possible explanation is that the β-function is energy dependent. As mentioned in Sec. II, the effect of the energy shift is to give rise to an additional orbit shift that is proportional to the dispersion function (to first order). This effect is accounted for in the fits. However changing the energy also causes the β-function to change; an effect that is not accounted for in the fits. We have made a rough estimation of this effect, and it gives a discrepancy of a few μm rms. One way to reduce this effect is to simultaneously change the RF frequency when a corrector is changed in order to keep the beam energy constant. At this time, we have not done that.

IV. ORBIT ERRORS IN SEXTUPOLES

As was mentioned previously if the orbit of the beam in the sextupoles is horizontally displaced from the magnetic center then there is a quadrupole component of the field. Here is the reason. The vector potential, A_z, of a sextupole is

$$A_z = -\frac{S}{3}\left(x^3 - 3xy^2\right) \tag{6}$$

where S is the integrated sextupole strength in units of m^{-2} and x and y are measured with respect to the magnetic center of the sextupoles. If there is a horizontal closed orbit distortion, x_0, in the sextupoles, then one can rewrite the vector potential as

$$A_z = -\frac{S}{3}\left[\left(x^3 - 3xy^2\right) - 3x_0\left(x^2 - y^2\right) - 3x_0^2 x - x_0^3\right] \tag{7}$$

where x and y are measured with respect to the beam closed orbit. The first term in equation 7 is the usual sextupole term but due to the horizontal offset in the closed orbit there is a quadrupole (second term) and dipole (third term) feed down component of the field. The vector potential, A_z, of a quadrupole is

$$A_z = -\frac{K}{2}\left(x^2 - y^2\right) \tag{8}$$

where K is the integrated quadrupole field in units of m^{-1}. Comparing equations 7 and 8 the equivalent quadrupole component, K_s, in a sextupole is

$$K_s = 2Sx_0 \tag{9}$$

Given the sextupole's integrated strength, S, and integrated gradient, K_S, measured with respect to the beam's closed orbit, one knows x_0, the position of the beam with respect to the magnetic center of the sextupole.

To determine x_0, first the response matrix with sextupoles turned on is fitted keeping the quadrupole gradients fixed to the value determined previously with sextupoles turned off. From this fit we determine the 48 K_s. Second the sextupole gradients, S, are determined by adjusting the sextupoles to correct the linear chromaticity to zero in the model. One

power supply powers all of the SF sextupoles and one power supply powers all of the SD sextupoles. In our fits we assumed one sextupole strength for all the 24 SF sextupoles and one sextupole strength for all the 24 SD sextupoles. Based upon similar assumptions made about the quadrupoles in the previous section, the assumption is made that there is little variation in S among the sextupoles in a family. Having values of K_s and S for each of the sextupoles, equation 9 is used to determine the offsets, x_0. The results are plotted in Fig. 7.

As seen in the figure, the offsets are rather large, as much as 1.5 mm in the SFs and 0.8 mm in the SDs. Also Fig. 7 shows that the beam is mostly radially outside of sextupole's magnetic center. The reason for the shift is due in part to the rf frequency not adjusted properly on the day this measurement was taken.

The offsets in the sextupoles resulted in an additional increase in the amplitude of beating of the β-function. As can be seen in Fig. 6 the rms perturbation of the β-function is 6% horizontally and 19% vertically. Even though there is some increase in the distortion of the β-function most of the distortion was a result of the mispowered quadrupoles.

How do we trust that we have found the actual offsets of the beam with respect to the magnetic center? We tested the fits by moving the orbit in the sextupoles by a known amount and checked to see if the change in the fitted offset before and after the orbit is moved correctly reflects the change in orbit. This is done by measuring and fitting three separate response matrices. First we measure an orbit response matrix with the sextupoles turned off and fit the quadrupole gradients in all the quadrupoles. Then we switch on the sextupoles. The sextupoles are powered so that the measured chromaticity is zero in both planes. Then we measure a second response matrix and fit the quadrupole gradients of the sextupoles. Next we distort the horizontal closed orbit by changing one horizontal corrector to give roughly a 1 mm change in the orbit peak-to-peak. To do this we changed the correctors excitation current by 3 Amps. A new response matrix is measured and the quadrupole gradients of the sextupoles are refitted.

After the response matrices are fit, the horizontal beam offset in the sextupoles is computed for each sextupole before and after the horizontal orbit is changed. The change in the

orbit is then just the difference between the horizontal offsets before and after the corrector was changed.

By modeling the orbit response matrices we can determine the change in orbit in a second way. From the fitted model we determine that a 3 Amp change in the corrector corresponded to a 0.2 mrad kick. Using the fitted model we can predict how much a 0.2 mrad corrector kick will change the closed orbit at the sextupoles.

So we determine the orbit change at the sextupoles in two ways: one by fitting the quadrupole gradient in the sextupoles and the other by fitting the gains of the correctors. A comparison of the two methods is shown in Fig. 8. For a 0.56 mm rms shift in orbit, the orbit changes at the sextupoles agree to within 75 μm. This gives us confidence that the absolute offset is found to reasonable accuracy ($\sim$100 μm).

There are two assumptions in the fit. One is that the each member of the sextupole family has the same integrated strength. As discussed earlier this is a reasonable assumption. The other assumption is that the gain of the corrector is determined correctly. As discussed in reference [4] the absolute gains of the correctors and the BPMs could both be off by a constant factor that can not be determined in the fit. The good agreement between the two methods suggests that the assumptions made about the magnet-to-magnet variation of the sextupoles in a family and the absolute corrector gain are good.

V. RESTORING THE PERIODICITY OF THE LATTICE

Once the real lattice is known it is then possible to adjust the quadrupoles to correct the optics and restore the lattice periodicity. Choosing how the quadrupoles get set depends on what is important. For instance it may be important to restore the β-function to restore the beam size back to ideal. Or it may be important to have the linear transfer functions between the sextupoles the same to restore the dynamic aperture [12]. Doing this may mean that the β-function may vary quite a bit from ideal. This happens in the situation that there is one large gradient error in the ring and it can't be corrected locally. In our case

we chose the following merit function: Adjust the quadrupoles to minimize the difference between the actual and ideal response matrix. Because we have distributed gradient errors this merit function effectively corrects both the β-beating and the transfer matrices between sextupoles.

Determining the quadrupole values that best correct the optics is also done with LOCO, and the algorithm is as follows. We have 49 individual parameters that can be adjusted to compensate the β-beating in the ring: each one of the QF and QD quadrupole magnets which can be adjusted individually and the QFA quadrupoles that can be adjusted as a group. (In principle we could also change the orbit in the sextupoles but this was not done.) Lets say that K_{q0} and K_{s0} are the ideal values for the quadrupoles and the sextupoles in the lattice (In the ideal lattice K_{s0}=0). Lets say that K_{q1} and K_{s1} are the actual values for the quadrupoles and the sextupoles in the lattice. If we could adjust each of these parameters individually we could restore the lattice to ideal.

But we are only able to adjust a subset of the parameters, namely the 49 mentioned above. In that case we fit the orbit response matrix with sextupoles on with only those quadrupole gradient parameters that we can adjust. We leave the gradients in the sextupoles zero in the fit model. We then find the variation in those 49 parameters that best reproduces the break in periodicity of the measured response matrix. We then adjust the quadrupole power supplies in the ring with just the opposite variation. A new set of response matrices are measured then and the model is refit. From this we compute the β-beating of the lattice and find that it has reduced to less than 1% RMS (see Fig. 9). Thus we have answered question 3 posed in the introduction. Now we move on to answer questions 4 and 5: What is the effect on the beam dynamics from the broken periodicity, and how does the behavior change when the optics are corrected?

VI. EFFECT OF PERIODICITY BREAKING ON INJECTION EFFICIENCY

Experimentally we found that correcting the optics dramatically improved our injection rates. To explain the experiment we first need to describe the injection process. An illustration of the injection process is given in Fig. 10. Plot (a) shows the situation before injection. The stored beam is centered in the ring with a magnetic septum located 21 mm horizontally inward (to the right). Plot (b) shows the situation during injection. The stored beam is bumped 15 mm inward towards the septum. At the same time the injected beam enters the ring on the opposite side of the septum. The duration of the bump lasts about 4 μ (a few turns) after which both the injected and the stored beam are clear (to the left) of the septum.

The storage ring acceptance drawn in Fig. 10 (a) and (b) is 15 mm. As plot (b) indicates, when the stored beam is locally bumped, the injected beam just falls inside the acceptance. As the bump or the aperture becomes smaller fewer injected particles are captured. Conversely, the amplitude of the bump can not be too large or the stored beam will strike the septum. This will cause some or all of the stored beam to be lost.

Before the optics of the lattice was corrected, we were experiencing a low injection efficiency. We suspected that this was due in part to a reduction in the transverse dynamic aperture resulting from the periodicity breaking. In order to get a reasonable injection rate we needed to create a distortion of the closed orbit of about 4 mm towards the septum (see Fig. 10 (c) and (d)). This indicated a smaller than expected acceptance. Putting in a 4 mm distortion in the orbit gave us the maximum injection efficiency. If we increased the amplitude of the bump the injection rate went down presumably because we were scraping some of the stored beam off the septum. We had a narrow region in parameter space where we could get a reasonable injection efficiency.

A comparison of the relative injection efficiency is made for the ring before and after the optics was corrected. The results can be seen in Fig. 11. Without changing the injector, the injection rate was measured as a function of the relative distance between the stored beam

and the injected beam. This was done by incrementally shifting the stored beam further toward the injected beam using a closed orbit bump. At each bump amplitude the measured injection efficiency is significantly better for the lattice with corrected optics.

Fig. 12 shows a numerical simulation of the dynamic aperture for the original fitted model and the fitted model after periodicity restoration. The only errors included in the model are the fitted gradient errors. There are no coupling or higher-order multipole errors included. Particles are tracked on-energy and without synchrotron oscillations for 512 turns or until lost. The dynamic aperture is substantially larger for the lattice with the corrected optics.

The dynamic apertures plotted in Fig. 12 are larger than the storage ring acceptances drawn in Fig. 10. The calculated apertures are probably larger than the actual ones due to the fact that we only included gradient errors in the machine. So there is some uncertainty about the absolute magnitude of the aperture. Nevertheless Fig. 12 demonstrates that there is a large reduction in the dynamic aperture for the uncorrected optics.

VII. EFFECT OF PERIODICITY BREAKING ON RESONANCE EXCITATION

In this section we show that the measured distortion of the beam tail distribution, resulting from unallowed resonances being excited, is reduced after the optics are corrected. When excited, structural resonances may alter the behavior of particles in the beams tail. Resonances may cause particles to increase and decrease their transverse amplitudes or to be trapped at large amplitudes (for instance particles may get trapped in resonance islands). Therefore by monitoring changes in the beam tails as the betatron tunes are varied it is possible to observe the onset of resonances.

The way in which we monitor the tails is by limiting the transverse physical aperture with a beam scraper and measuring the beam lifetime as a function of the betatron tunes. If resonances are present in the vicinity of the tunes and there is a change in the beam shape, there will be a changing in the number of particles that hit the scraper when they

make large amplitude excursions resulting in a change in the beam lifetime. Thus if we vary the betatron tunes while simultaneously observing the beam lifetime we will see the lifetime drop or rise when we move onto excited resonances. The experimental technique is very similar to that which was used in VEPP-4 [13] to measure the effect of the beam-beam force on the tails of the beam. A beam loss monitor is located just down-stream of a horizontal and vertical beam scraper and the loss monitor detects bremsstrahlung being emitted from the scraper. The count rate detected is proportional to the rate at which particles hit the scraper and is linearly related to beam lifetime. Therefore by observing the change in the ratio of the beam current to the detector count rate as a function of betatron tune we can observe a change in lifetime and thus the onset of resonance excitation.

Our experimental procedure was the following. We would first change the tunes by changing two families of quadrupoles, QF and QD, according to a previously measured transfer matrix. After the quadrupole fields have settled we measured the beam current and the count rate in the detector for a 1 second interval. (The whole process is automated and takes about 2 seconds per tune point.) Then move on to the next tune. In order to check how well the predicted tunes agree with the measured tunes we would periodically measure the tunes.

There are two advantages of measuring the count rate and current verses a direct measurement of the lifetime. First the measurment is fast. We can scan nearly 2000 tune values per hour. The second advantage is the fluctuation in the detector count rate is small (roughly 3%) which is due to the large detector count rate ($\sim$ 1 KHz for a 10 hour lifetime with a beam current of 5 mA). The combination of a fast measurement and high sensitivity makes this technique more attractive than measuring the beam lifetime directly.

A. Before periodicity was restored

We chose to scan in a region of tune space where two resonances are present: $5\nu_x = 72$ (allowed by periodicity) and $3\nu_x = 43$ (unallowed by periodicity). The first scan was made

with the lattice before the periodicity was restored. The scan covered a rectangular region in tune space ($14.3 < \nu_x < 14.45$ and $8.1 < \nu_y < 8.15$). Within this region we scanned 101 horizontal tune values by 6 vertical tune values ($\Delta\nu_x$ steps of 0.0015 by $\Delta\nu_y$ steps of 0.01).

Fig. 13 (top row) shows the results of the scan. Three resonances can be seen in the scan:

$$5\nu_x = 72 \qquad \text{allowed}$$
$$3\nu_x = 43 \qquad \text{unallowed}$$
$$2\nu_x + \nu_y = 37 \quad \text{unallowed}$$

In particular it is clear from Fig. 13 (top row) that resonance $3\nu_x = 43$ is largely excited.

B. After Periodicity was Restored

The second scan was made after we restored the periodicity and the results can be seen in Fig. 13 (bottom row) . Looking at the figure it is clear that the resonance $3\nu_x = 43$ has been greatly suppressed down below the level of the allowed resonance, $5\nu_x = 72$. One can also see from the figure that the coupling resonance $2\nu_x + \nu_y = 37$ seems to be of the same amplitude as before. This is not surprising considering that this is a coupling resonance and when the periodicity was restored we made no attempt to correct the coupling in the machine. In Fig. 14 a two dimensional plot is shown where the vertical axis is count rate divided by current and the bottom axis is horizontal tune. The vertical tune is kept roughly constant at $\nu_y = 8.15$ In this picture we can more clearly see the relative amplitudes of the various resonances. A dramatic reduction in the $3\nu_x$ resonance can be seen after periodicity is restored.

We also made a larger scan of the tune region ($14.1 < \nu_x < 14.45$ and $8.1 < \nu_y < 8.4$). We found that in the case of the lattice with periodicity restored we are easily able to move over this large region of tunespace while observing very few resonances being excited. The results of the tunescan are displayed in Fig. 15. Besides the resonances mentioned one also

sees the coupling resonance ($\nu_x = \nu_y$). It is remarkable how clean the picture looks and how easily one can move over the tune space when one has a periodicitic machine.

This is not the case with the lattice before the periodicity is broken. We found that the beam was not stable in many areas of the scanned tunespace. In fact we found that there were a number of areas in tunespace that could not be scanned without loosing the beam.

C. Interpretation of the tunescan data

The effects of periodicity breaking on the behavior of the tails at different tunes are illustrated with the help of phase space plots of the fitted lattices. Fig. 16 shows the horizontal phase spaces next to the $3\nu_x = 43$ and $5\nu_x = 72$ resonances. The left side shows the phase space of the optics before periodicity was restored, the right side shows the phase space of the ideal optics.

Let us first consider the $5\nu_x$ resonance (lower figures): The resonances islands are even visible in the unperturbed case, as expected from the resonance condition of the periodicitic machine. These islands remain unchanged when breaking the periodicity. Only the outer part of the phase space is distorted by the $8\nu_x = 115$ resonance. In the vicinity of the $3\nu_x$ resonance the situation is completely different. Whereas in the unperturbed case there is no distortion at all, the inner phase space becomes completely distorted by the islands of the 3rd integer resonance when the periodicity is broken.

We expect that with islands in the phase space particles can get captured in the tails either through gas scattering or intrabeam scattering. This distorts the distribution of the beam leading to an increase in the beam loss rate. From the phase space pictures in Fig. 16 we expect that the tail distributions and the beam loss rate in the vicinity of the $5\nu_x$ resonance would remain roughly the same before and after periodicity was restored. While in the vicinity of the $3\nu_x$ resonance the tail distributions and count rate would be higher before the periodicity was restored. This is consistent with what we observed experimentally (see Fig. 14). A close observation of Fig. 14 reveals that even after the periodicity was restored

there is still a small increase in count rate near the $3\nu_x$ resonance. This indicates that periodicity is not perfectly restored.

D. Beam profile monitor

We have the ability to observe the beam distribution with a beam profile monitor. This monitor images the synchrotron radiation that is emitted from a bending magnet and represents roughly a one-to-one image of the beam. An image of the beam near the $3\nu_x$ resonance can be seen in Fig. 17 before (left) and after (right) the periodicity was restored. What we see is that in the lattice before the periodicity was restored the beam "splits" into several spots. However that was not the case after the periodicity was restored.

E. Interpretation of the beam profile measurement

Again a phase space plot of the fitted lattice is used to help us understand the image. In Fig. 18 we have plotted the horizontal phase space of the lattice without the periodicity restored. The tracking point of the phase space corresponds to the observation point of the beam. As we expect there are three islands in the phase space. One can imagine that if the islands are populated the projection onto the normal space would look something like the image. The reason that one sees only three spots and not four is that when one projects the phase space onto the x-axis two islands overlap. The phase space plot is only meant to serve as a qualitative understanding of the image. We make no quantitative statements about the distribution.

VIII. CONCLUSION

The periodicity of the linear lattice is clearly important for the ALS. The actual linear lattice is accurately determined by analyzing orbit response matrices. From this analysis we have found power supply errors and orbit offsets in sextupoles which lead to a beating

of the vertical β-function of 19%. Knowing the errors in the machine we then adjusted quadrupoles in the machine to restore the lattice periodicity. After the quadrupoles were adjusted, beating of the β-function was reduced to less than 1%.

We find that by restoring the lattice periodicity there have been several beneficial effects on the machine performance. First, the injection efficiency is improved. Second, the excitation of unallowed nonlinear resonances is suppressed. As a result we are able to tune the machine anywhere (except near integer and half integer resonances) with stable beam. Finally we find that by restoring the lattice periodicity the beam profile remains nearly constant near unallowed resonances.

IX. ACKNOWLEDGEMENTS

The authors would like to thank the staff at the ALS, particularly Alan Jackson for his encouragement and support of the work and with whom we had many interesting discussions. Also we would like to thank Alan for making high precision power supply measurements. We wish to thank Gary Krebs for setting up the radiation monitors used in the tunescan experiments. We wish to thank Greg Portmann for helping to automate the tunescan measurements. Also we wish to thank Greg, Jim Hinkson and Jim Johnson for reducing the noise levels of the BPMs. We would like to thank Sasha Zholents for suggesting the tunescan technique for measuring resonance excitation. We wish to thank Sam Krinsky at BNL for encouraging one ot the authors (J.S.) to participate in this work. We would also like to thank Martin Lee, Jeff Corbett at SLAC for interesting discussions. This work was supported by the Director, Office of Energy Research, Office of Basic Energy Sciences, Materials Sciences Division of the U.S. Department of Energy, under Contract No. DE-AC03-76SF00098.

REFERENCES

[1] Lawrence Berkeley National Laboratory Report No. LBNL/PUB-5172, 1986, (unpublished).

[2] W. J. Corbett, M. Lee, and V. Ziemann, in *Proceedings of the 1993 Particle Accelerator Conference, Washington*, p. 108.

[3] J. Safranek, in *Proceedings of the 1995 Particle Accelerator Conference, Dallas*, p. 2817.

[4] J. Safranek, Nucl. Inst. and Meth. **A388**, 27 (1997).

[5] J. Bengtsson and M. Meddahi, in *Proceedings of the 1994 Particle Accelerator Conference, Berlin*, p. 1021.

[6] D. Robin, J. Safranek, G. Portmann, and H. Nishimura, *Proceedings of the 1996 Particle Accelerator Conference, Barcelona*, p. 971.

[7] M. P. Woodley *et al.*, Stanford Linear Accelerator Conference Report No. SLAC/PUB 3086, 1983, (unpublished).

[8] Alan Jackson (private communication).

[9] E. Ciapala *et al.*, IEEE Trans. Nucl. Sci., NS **26**, No. 3, 3571 (1979).

[10] Advanced Light Source Parameter List, Edition VIII, 1992, (unpublished).

[11] Measurements made by Alan Jackson.

[12] J. Bengtsson and E. Forest, *AIP Conference Proceedings No. 255, 1991*, p. 229.

[13] A. B. Temnykh, in *Proceedings of the IX ALL - Union Meeting on Accelerators of Charged Particles, Dubna,* 1984, v. 2, p. 163.

FIGURES

FIG. 1. Typical ALS Storage Ring sector.

FIG. 2. Resonance Diagram: All betatron resonances up to 5th order (left), all "allowed" resonances up to 5th order with 12-fold periodicity (right).

FIG. 3. A comparison of 1 column of the response matrix (+) with the ideal lattice and with the lattice after fitting.

FIG. 4. A comparison of the relative variation of QD quadrupole strengths as measured with a current monitor and fitted response matrix.

FIG. 5. Horizontal and vertical β-beating with sextupoles turned off.

FIG. 6. Horizontal and vertical β-beating with sextupoles turned on.

FIG. 7. Horizontal offset of the electron beam to the sextupole magnetic center for each of the 24 SF and SD sextupoles.

FIG. 8. Comparison of two methods for determining an orbit change in the ALS when one corrector is changed. Method 1 (solid line): Use the fitted model of the ring and the fitted gain of the corrector to calculate the orbit shift. Method 2 (circles): Use the calculated orbit change from the difference in the quadrupole gradients in the sextupoles.

FIG. 9. Horizontal and vertical β-beating after the optics are corrected.

FIG. 10. Injection process: (a) before injection with a 15 mm acceptance, (b) during injection with a 15 mm acceptance, (c) before injection with a 10 mm acceptance and a 4 mm closed orbit offset, and (d) during injection with a 10 mm acceptance and a 4 mm closed orbit offset.

FIG. 11. A comparison of the injection rate, before and after the optics were corrected, as a function of the orbit distortion in the injection straight. (More negative means closer to the injection septum.)

FIG. 12. A comparison of the calculated dynamic aperture before and after the optics are corrected

FIG. 13. Tunescans before (top) and after (bottom) the optics are corrected. At each horizontal and vertical tune, the count rate (as measured in a gamma counter) divided by beam current is plotted. The two data sets are drawn in both a hill (left) and a contour (right) plot. All resonances up to 5th order are drawn on the contour plot.

FIG. 14. Horizontal tunescans before (top) and after (bottom) the optics are corrected. The vertical tune is kept constant at 8.15. At each horizontal and vertical tune, the count rate (as measured in a gamma counter) divided by beam current is plotted.

FIG. 15. Larger area tunescans of the lattice after the optics are corrected. At each horizontal and vertical tune, the count rate (as measured in a gamma counter) divided by beam current is plotted. Data is drawn as a hill plot (left) and as a countour plot (right). All "allowed" resonances up to 5th order are plotted (solid line). The resonance $\nu_x = 43$ is plotted as a dashed line.

FIG. 16. Comparison of the horizontal phase space for an ideal machine (left) and one with uncorrected optics (right). The plots are made with the model tuned in the vicinity of the $3\nu_x = 43$ (upper) and the $5\nu_x = 72$ (lower) resonances.

FIG. 17. Synchrotron radiation image of the beam near the 3 ν_x resonance. Left is the situation before the optics are corrected and right is the situation after the optics are corrected. (The plane of the camera is rotated with respect to the plane of the beam. Also there is a distortion in the light optics in the vertical plane that is responsible fo the images vertical asymmetry.

FIG. 18. Horizontal phase space of the lattice plotted at the observation point. Lattices are tuned to $\nu_x = 14.3338$ and $\nu_y = 8.15$. Left plot shows the phase space with the uncorrected optics. Right plot shows the phase space for the ideal machine.

TABLES

TABLE I. Variation in quadrupole field strengths determined by fitting orbit response matrices

Quadrupole Family	rms Variation
QF	0.20%
QD	0.63%

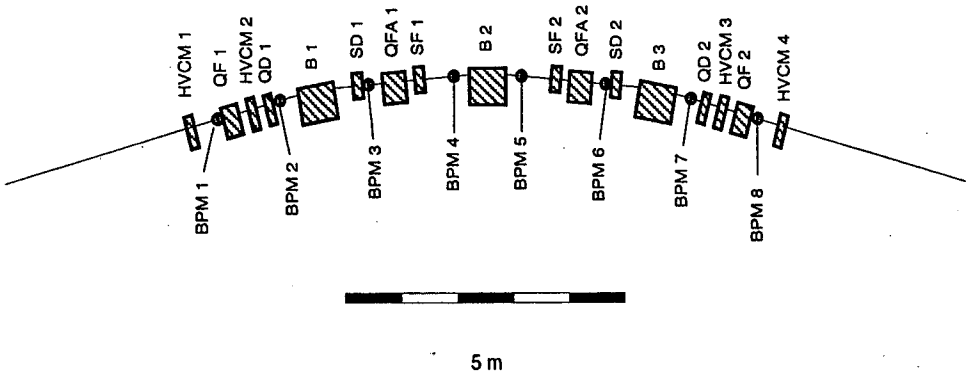
HVCM 1
QF 1
HVCM 2
QD 1
B 1
SD 1
QFA 1
SF 1
B 2
SF 2
QFA 2
SD 2
B 3
QD 2
HVCM 3
QF 2
HVCM 4
BPM 1
BPM 2
BPM 3
BPM 4
BPM 5
BPM 6
BPM 7
BPM 8
5 m

FIG 1

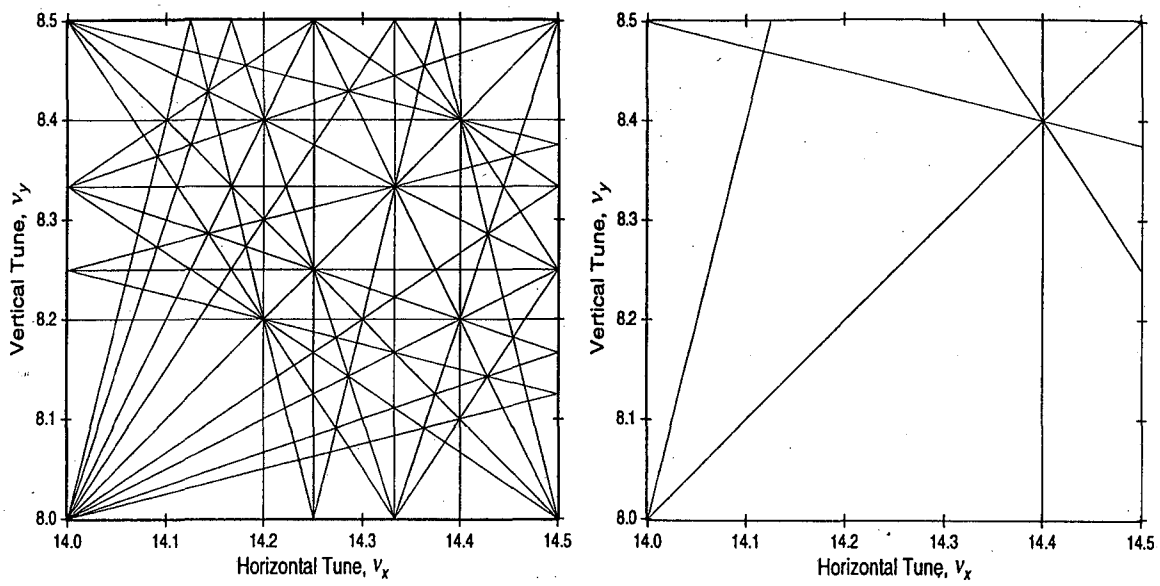
8.5
8.4
8.3
8.2
8.1
8.0
Vertical Tune, ν_y
14.0
14.1
14.2
14.3
14.4
14.5
Horizontal Tune, ν_x
8.5
8.4
8.3
8.2
8.1
8.0
Vertical Tune, ν_y
14.0
14.1
14.2
14.3
14.4
14.5
Horizontal Tune, ν_x

FIG 2

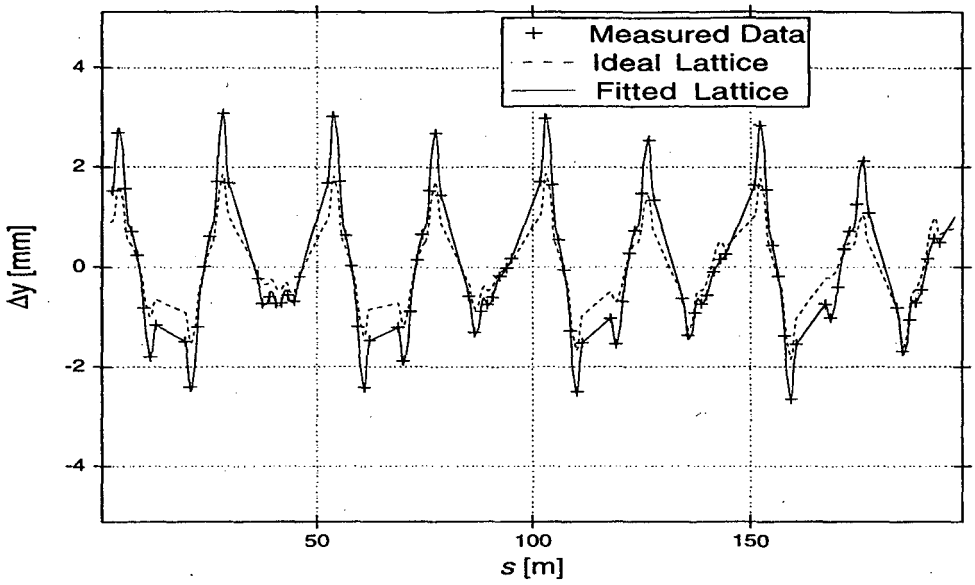
Measured Data
Ideal Lattice
Fitted Lattice
Δy [mm]
4
2
0
-2
-4
50
100
150
s [m]

FIG 3

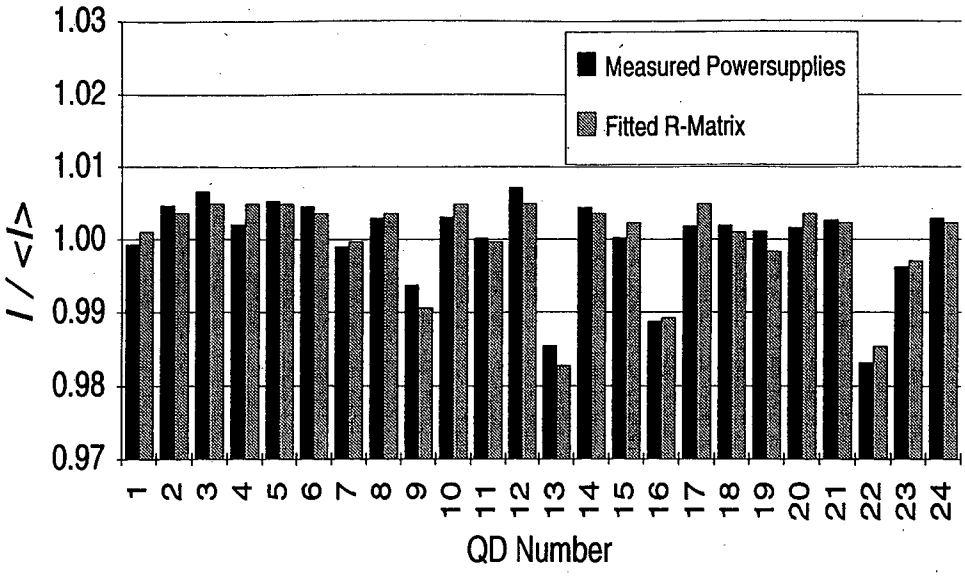
1.03
1.02
1.01
1.00
0.99
0.98
0.97
I / <I>
Measured Powersupplies
Fitted R-Matrix
1 2 3 4 5 6 7 8 9 10 11 12 13 14 15 16 17 18 19 20 21 22 23 24
QD Number

FIG 4

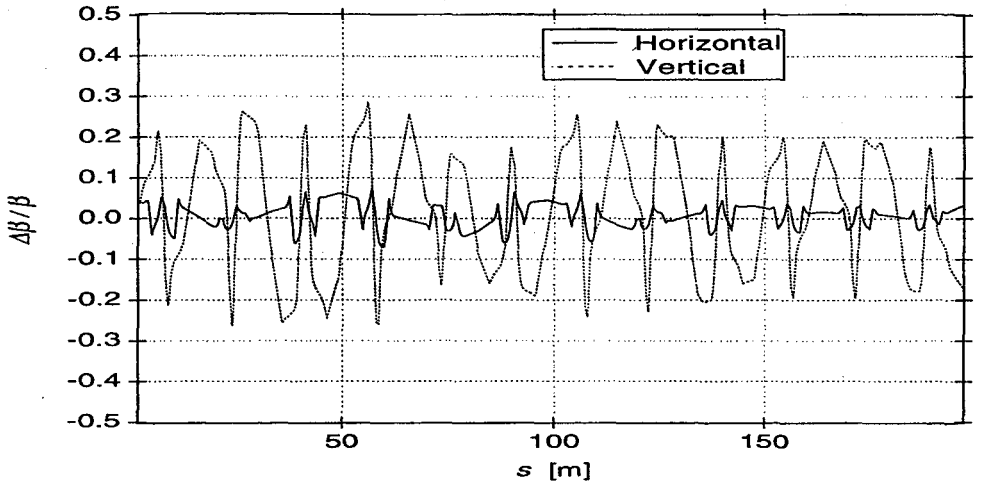
Horizontal
Vertical
0.5
0.4
0.3
0.2
0.1
0.0
-0.1
-0.2
-0.3
-0.4
-0.5
Δβ/β
50
100
150
s [m]

FIG 5

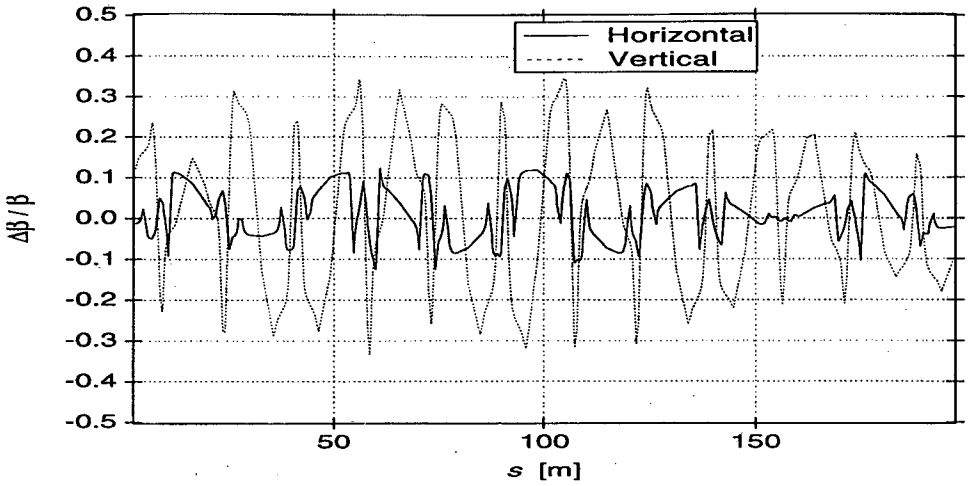
Horizontal
Vertical
0.5
0.4
0.3
0.2
0.1
0.0
-0.1
-0.2
-0.3
-0.4
-0.5
Δβ / β
50
100
150
s [m]

FIG 6

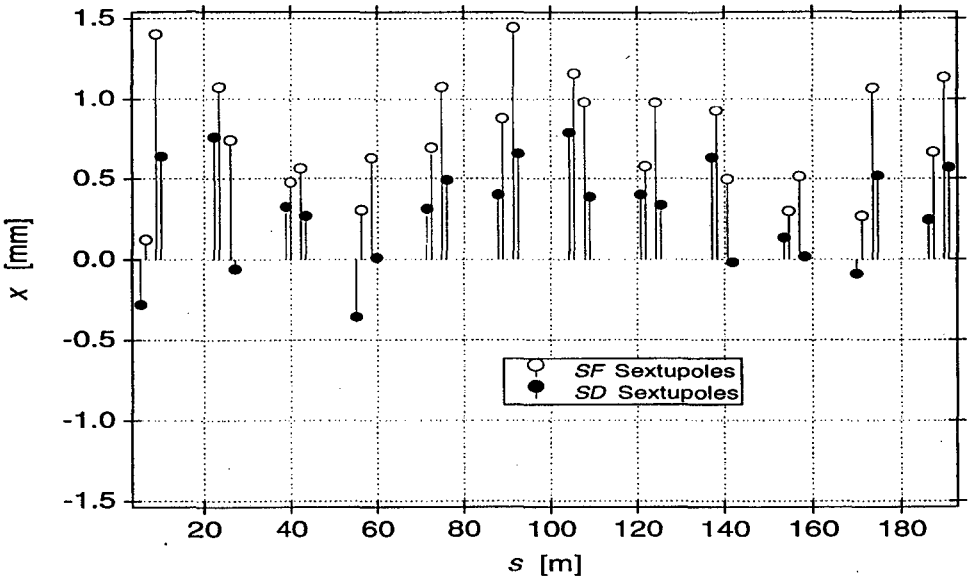
1.5
1.0
0.5
0.0
-0.5
-1.0
-1.5
x [mm]
20
40
60
80
100
120
140
160
180
s [m]
SF Sextupoles
SD Sextupoles

FIG7

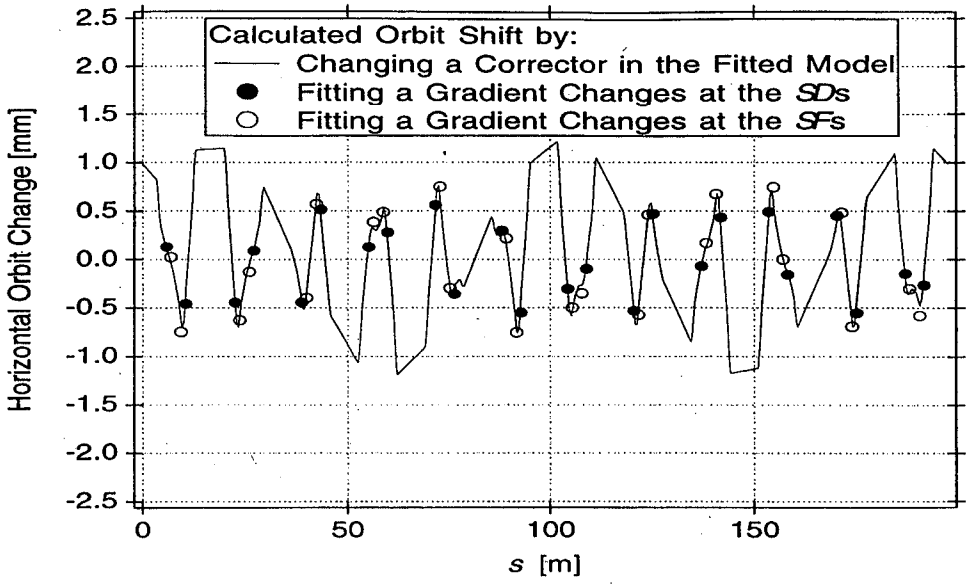
Calculated Orbit Shift by:
Changing a Corrector in the Fitted Model
Fitting a Gradient Changes at the SDs
Fitting a Gradient Changes at the SFs
Horizontal Orbit Change [mm]
2.5
2.0
1.5
1.0
0.5
0.0
-0.5
-1.0
-1.5
-2.0
-2.5
0
50
100
150
s [m]

FIG 8

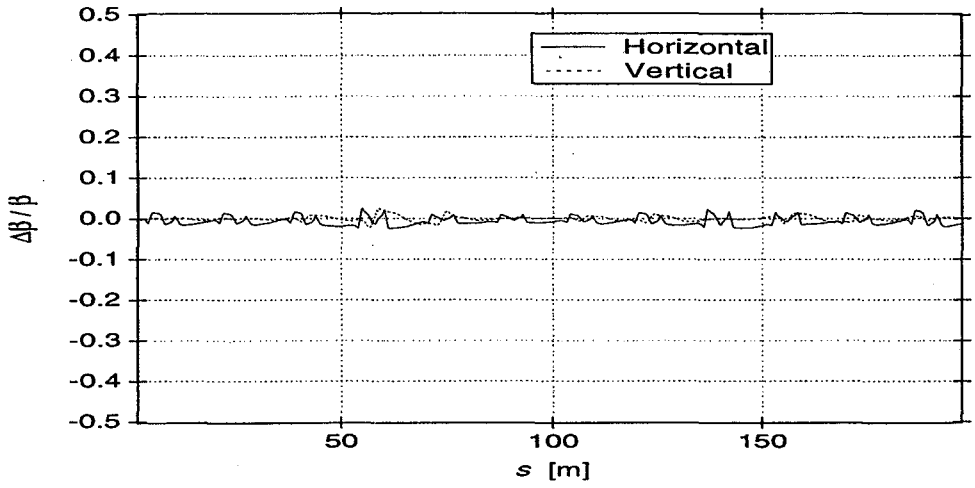
0.5
0.4
0.3
0.2
0.1
0.0
-0.1
-0.2
-0.3
-0.4
-0.5
Δβ/β
50
100
150
s [m]
Horizontal
Vertical

Fig 9

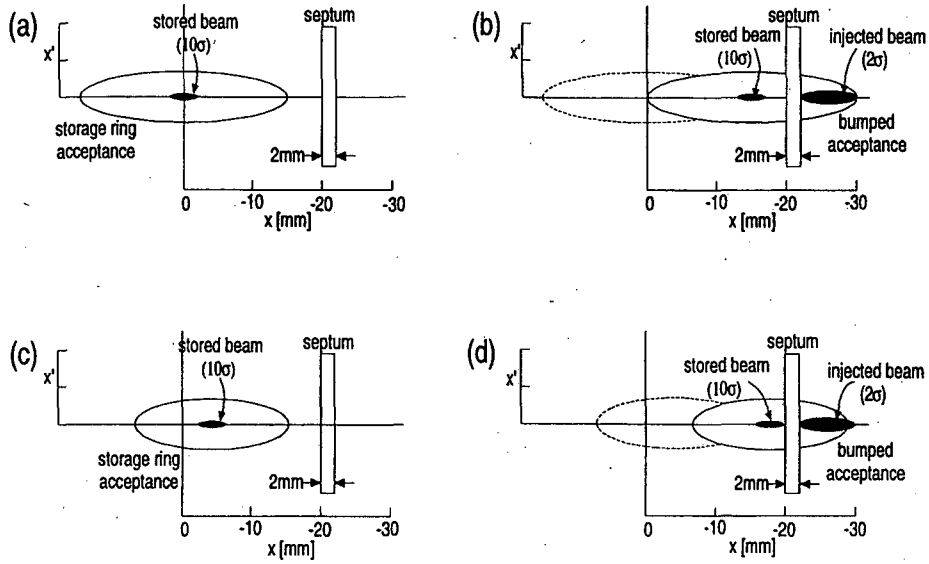
(a)
x'
stored beam
(10σ)
septum
storage ring
acceptance
2mm
0
-10
-20
-30
x [mm]
(b)
x'
septum
stored beam
(10σ)
injected beam
(2σ)
bumped
acceptance
2mm
0
-10
-20
-30
x [mm]
(c)
x'
stored beam
(10σ)
septum
storage ring
acceptance
2mm
0
-10
-20
-30
x [mm]
(d)
x'
septum
stored beam
(10σ)
injected beam
(2σ)
bumped
acceptance
2mm
0
-10
-20
-30
x [mm]

FIG 10

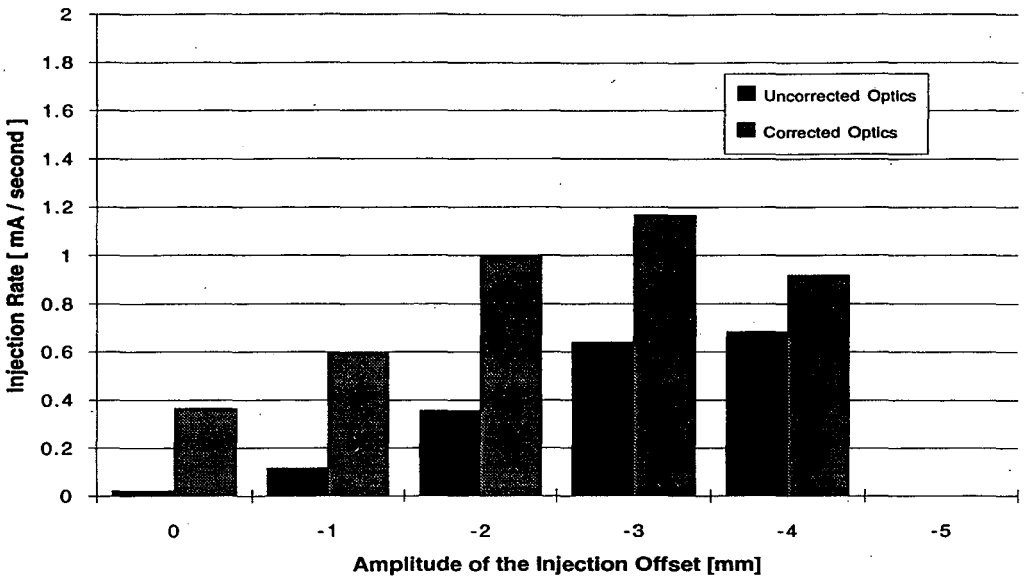
Injection Rate [mA / second]
2
1.8
1.6
1.4
1.2
1
0.8
0.6
0.4
0.2
0
Uncorrected Optics
Corrected Optics
0
-1
-2
-3
-4
-5
Amplitude of the Injection Offset [mm]

FIG 11

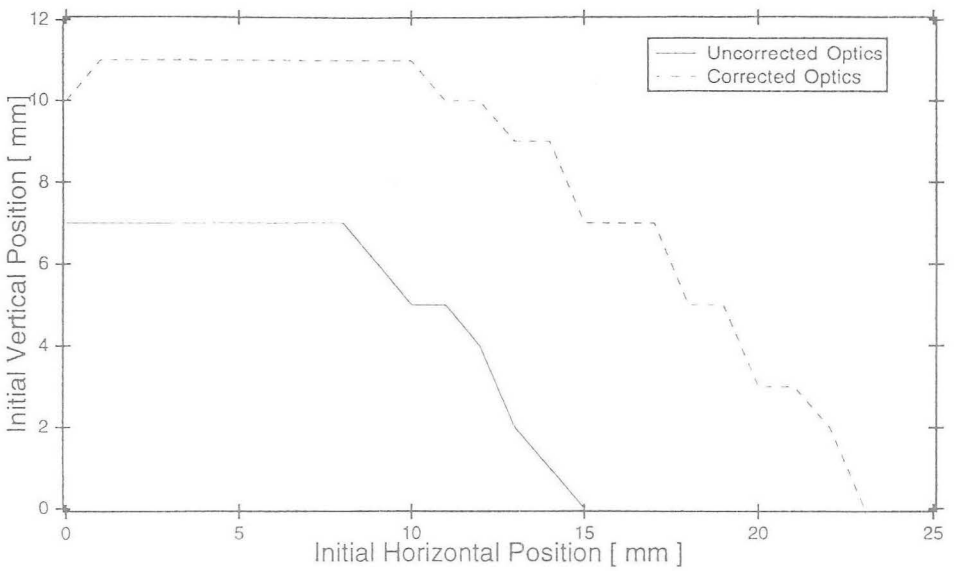
Uncorrected Optics
Corrected Optics
Initial Vertical Position [mm]
Initial Horizontal Position [mm]
0
2
4
6
8
10
12
0
5
10
15
20
25

Fig 12

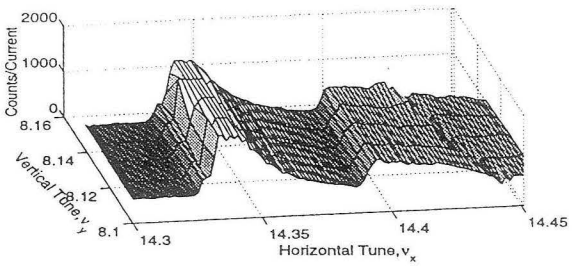
Counts/Current
2000
1000
0
8.16
8.14
8.12
8.1
Vertical Tune, ν_y
14.3
14.35
14.4
14.45
Horizontal Tune, ν_x

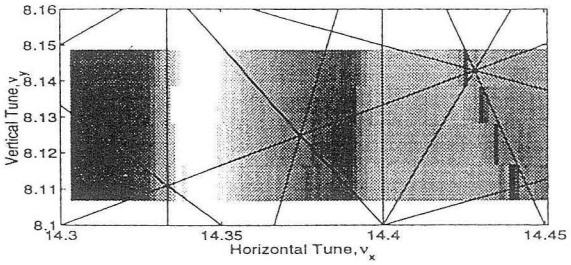
8.16
8.15
8.14
8.13
8.12
8.11
8.1
Vertical Tune, ν_y
14.3
14.35
14.4
14.45
Horizontal Tune, ν_x

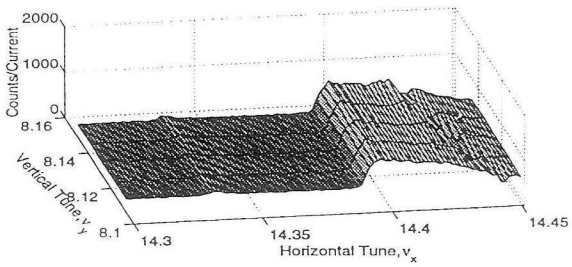
Counts/Current
2000
1000
0
8.16
8.14
8.12
8.1
Vertical Tune, ν_y
14.3
14.35
14.4
14.45
Horizontal Tune, ν_x

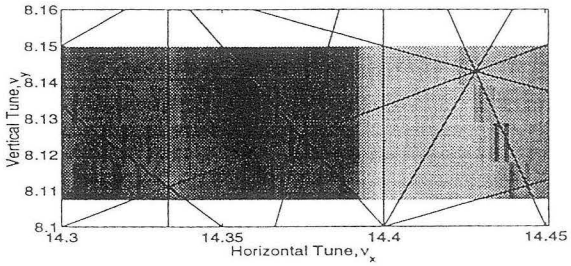
8.16
8.15
8.14
8.13
8.12
8.11
8.1
Vertical Tune, ν_y
14.3
14.35
14.4
14.45
Horizontal Tune, ν_x

FIG 13

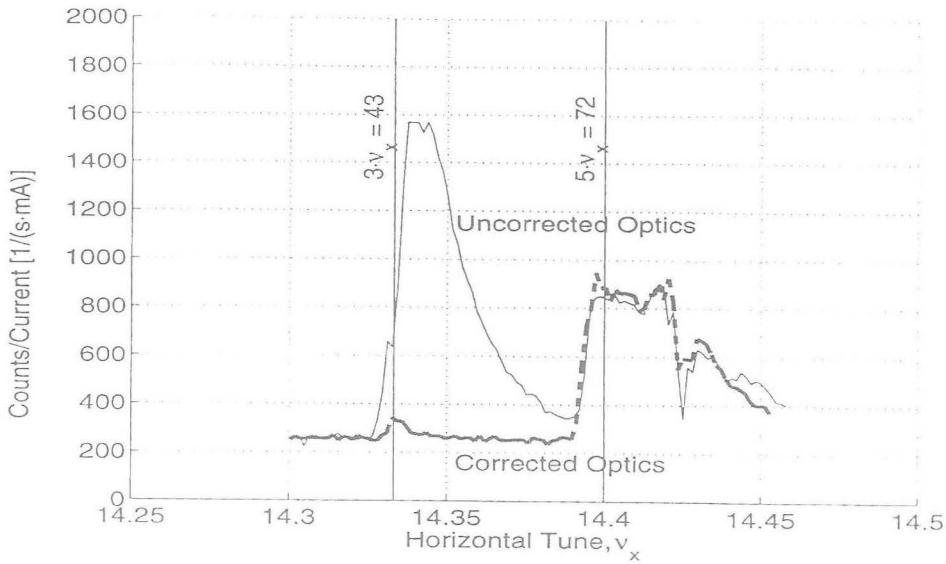
2000
1800
1600
1400
1200
1000
800
600
400
200
0
Counts/Current [1/(s·mA)]
3·ν_x = 43
5·ν_x = 72
Uncorrected Optics
Corrected Optics
14.25
14.3
14.35
14.4
14.45
14.5
Horizontal Tune, ν_x

FIG 14

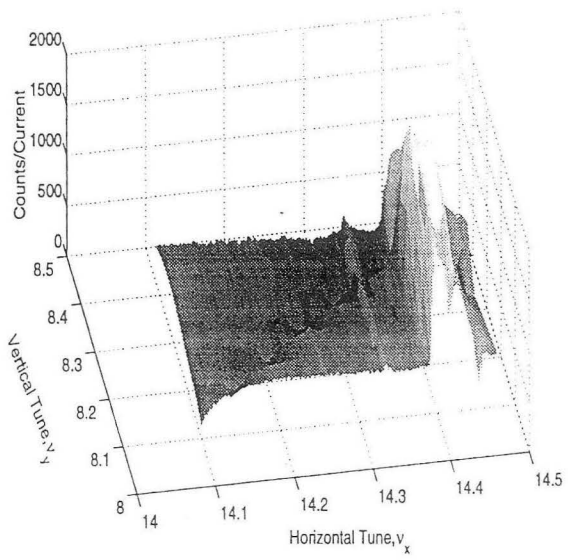
2000
1500
1000
500
0
Counts/Current
8.5
8.4
8.3
8.2
8.1
8
Vertical Tune, ν_y
14
14.1
14.2
14.3
14.4
14.5
Horizontal Tune, ν_x

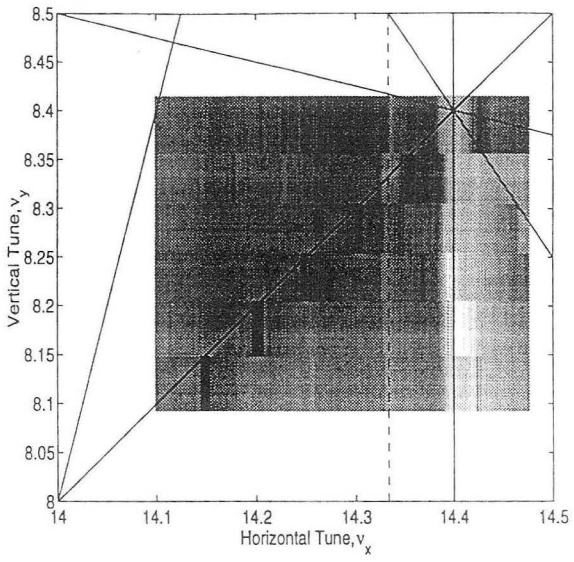
8.5
8.45
8.4
8.35
8.3
8.25
8.2
8.15
8.1
8.05
8
Vertical Tune, ν_y
14
14.1
14.2
14.3
14.4
14.5
Horizontal Tune, ν_x

F1615

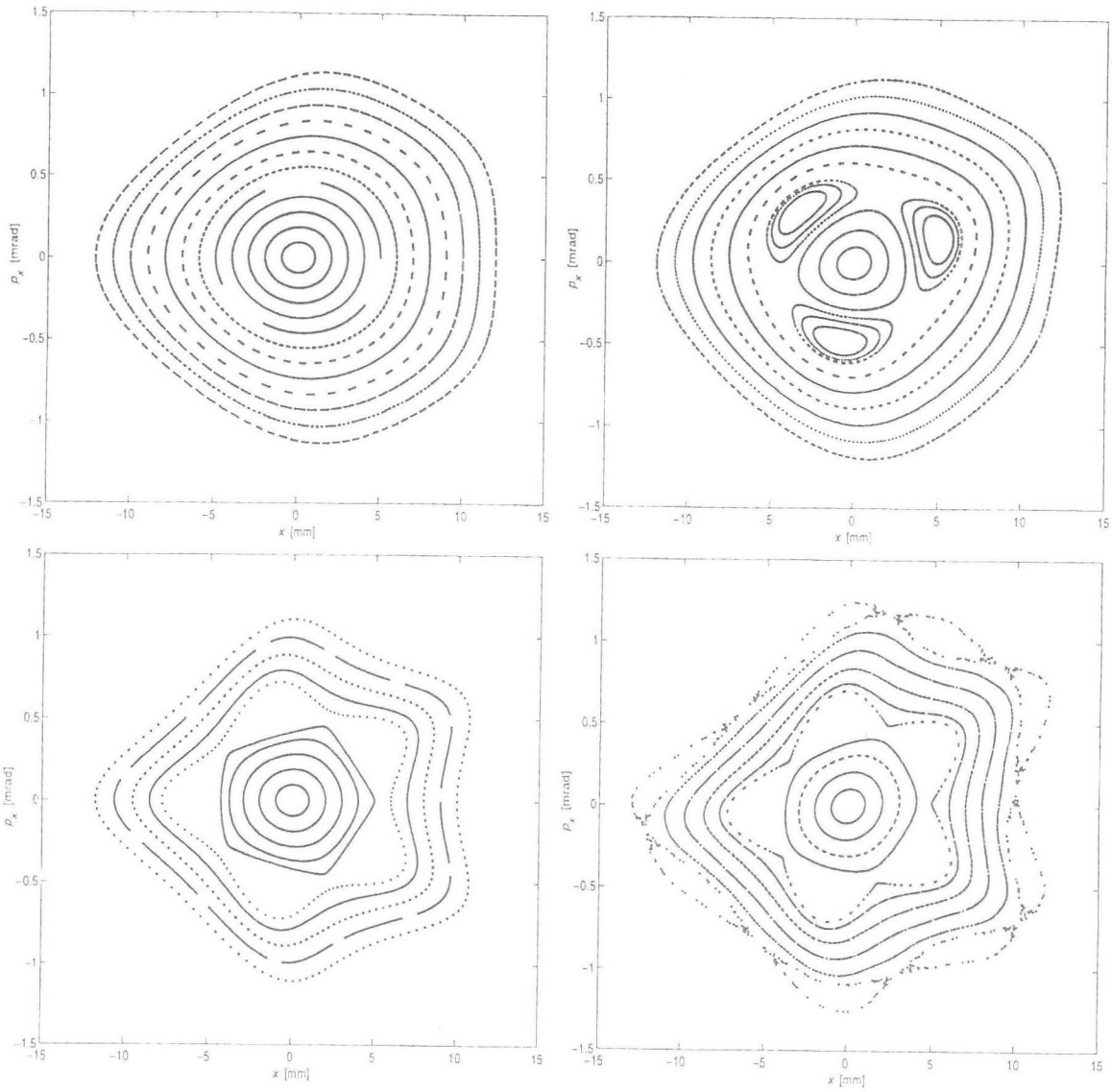

FIG 16

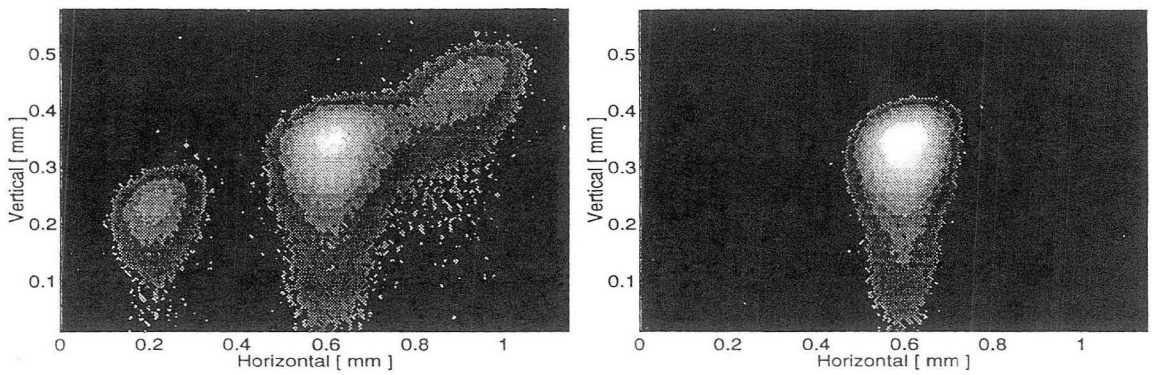
Vertical [mm]
0.5
0.4
0.3
0.2
0.1
0
0.2
0.4
0.6
0.8
1
Horizontal [mm]
Vertical [mm]
0.5
0.4
0.3
0.2
0.1
0
0.2
0.4
0.6
0.8
1
Horizontal [mm]

F16 17

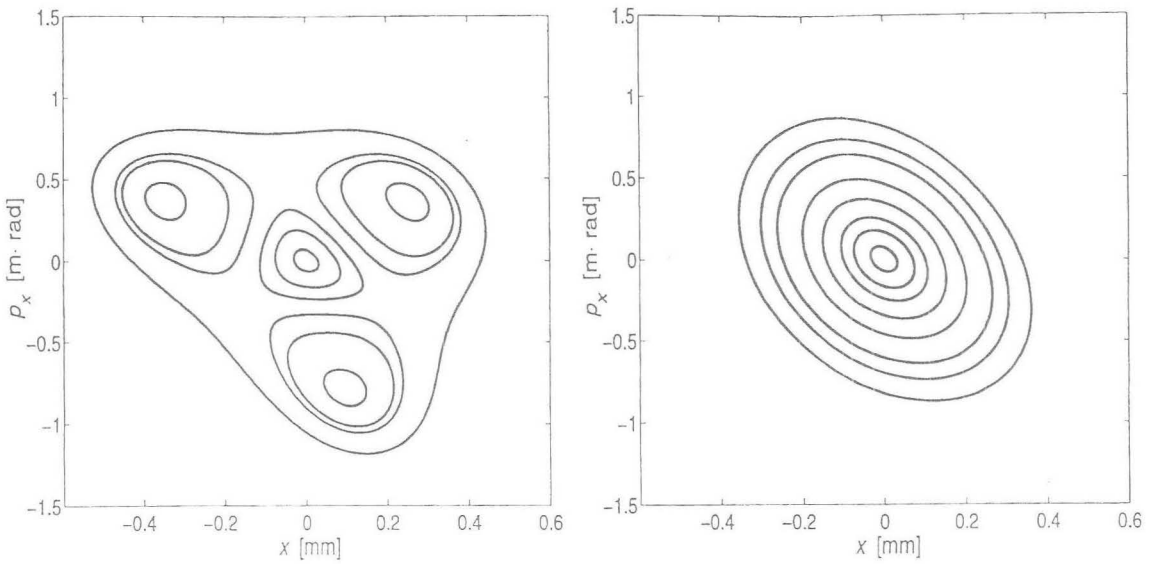

FIG 18

Ernest Orlando Lawrence Berkeley National Laboratory
One Cyclotron Road | Berkeley, California 94720

Prepared for the U.S. Department of Energy under Contract No. DE-AC03-76SF00098